

Additivity of the magneto-optic Kerr signal in ultrathin Fe(110)/Ag(111) superlattices

Z. Q. Qiu, J. Pearson, and S. D. Bader

Material Science Division, Argonne National Laboratory, Argonne, Illinois 60439

(Received 9 September 1991)

Fe(110)/Ag(111) superlattices were fabricated by molecular-beam epitaxy and investigated by means of the surface magneto-optic Kerr effect (SMOKE). Reflection high- and low-energy electron diffraction and Auger spectroscopy were used to determine that both Fe(110) on Ag(111) and Ag(111) on Fe(110) grow epitaxially. *In situ* SMOKE measurements were made as a function of the number of bilayers for four superlattice samples with bilayer thicknesses ranging from 19 to 25 Å. We find that the Kerr signal initially depends only on the total thickness of Fe and is independent of the intervening Ag layers. This result confirms that anticipated from a general macroscopic formalism evaluated in the thin-film limit.

I. INTRODUCTION

Artificially layered magnetic superlattices have attracted great interest in recent years.¹ A primary motivation is that the superlattice structure provides the possibility of combining desirable magnetic, structural, and optical properties to explore basic and applied issues.² The timeliness of the efforts is due to the recent development of advanced growth and characterization techniques applicable to thin films, as well as magnetic probes, such as Mössbauer spectroscopy³ and the surface magneto-optic Kerr effect⁴ (SMOKE). SMOKE, in particular, has the advantage of ease of operation and the potential for developing new magneto-optic storage materials.⁵

The basic principal of SMOKE is that the magnetization in magnetic material gives rise to nonzero off-diagonal elements in the dielectric tensor and rotates the plane of polarization of incident light upon reflection from the surface of the material. Thus, by detecting the component perpendicular to the incident polarization plane, the magnetization can be detected with sensitivity in the monolayer-thickness range. In the present work, we will apply the SMOKE technique to study Fe/Ag multilayers, which serve as a prototype for metallic magnetic-nonmagnetic superlattices.

The SMOKE signal from a superlattice depends on factors other than magnetic properties, such as the refractive indices and thicknesses of the individual component layers, the multilayer stacking sequence, etc.^{6,7} Great effort has been taken to calculate the SMOKE signal in multilayer systems.⁸⁻¹¹ In metallic films, because of the absorption of light in metals, the incident light can only penetrate a finite depth into the film. For example, the penetration depth of He-Ne laser light in most metals is ~ 100 – 200 Å, which is much less than the wavelength of the incident light ($\lambda = 6328$ Å). In such a situation, the phase difference of the incident light while traveling in the film is so small that the interference effect between individual layers can be ignored. As a result, one often can apply the thin-film approximation to simplify the calculation.¹² In the present work we present experimental results for the Fe/Ag-multilayer system and compared the results with that calculated from the magneto-optic for-

malism of Zak *et al.*¹¹ to test the expectation of an additivity law in the thin-film approximation.¹² The law states that the Kerr signal of the superlattice consists of a sum over the magnetic layers of the individual Kerr signals, without regard to the intervening nonmagnetic layers.

II. EXPERIMENT

A. Growth and characterization of the Fe(110)/Ag(111) superlattices

The Fe(110)/Ag(111) superlattices were fabricated by molecular-beam epitaxy (MBE) in an ultrahigh vacuum (UHV) system of base pressure 1×10^{-10} Torr. The system is equipped with reflection high-energy electron diffraction (RHEED), low-energy electron diffraction (LEED), Auger electron spectroscopy based on a hemispherical analyzer with a 140-mm mean radius, Ar-ion sputtering, and a split-coil UHV-compatible superconducting magnet.

The substrate used was cleaved mica that was first ultrasonically cleaned in methanol before introduction into UHV. The mica was annealed in UHV at 700 K for 12 h, and then a Ag(111) base layer was deposited onto the mica at a rate of ~ 0.5 Å/min from a Ag foil in an alumina crucible while the mica was held at 450 K. After ~ 1500 Å of Ag was deposited, the surface was sputtered by 5-keV Ar⁺ ions for a few minutes and annealed at 900 K for half an hour; then the film was cooled back down to 450 K and another 100–200 Å of Ag was homoepitaxially grown onto the Ag. After this process, the RHEED and LEED patterns indicated that a flat Ag(111) surface was achieved.¹³ From the high-quality RHEED pattern (with the beams in a semicircle and clear Kikuchi lines in the background) and sharp LEED beams, we estimate that the roughness of the Ag(111) surface is on an atomic scale. The Fe(110) films was deposited onto the Ag(111) surface from an Fe foil in an alumina crucible; the deposition rate was 0.1 Å/min and the substrate temperature was again 450 K. The pressure during the growth process remained below 3×10^{-10} Torr. The lattice mismatch between the $[\bar{1}10]$ axis of Fe and the $[\bar{1}10]$ axis of Ag is

$\sim 1\%$, and the misfit between the $[\bar{1}10]$ axis of Fe and the $[11\bar{2}]$ axis of Ag is $\sim 18\%$. Thus, the $[001]$ axis of Fe(110) will coincide with the $[1\bar{1}0]$, or $[0\bar{1}1]$, or $[10\bar{1}]$ axes of Ag to result in three growth directions of Fe(110) on Ag(111). This has been confirmed recently by an STM study on a similar system: Fe(110) on Au(111).¹⁴ The RHEED and LEED patterns identified the resultant structure as single-crystalline Fe(110), as we recently reported in Ref. 13. Four superlattice systems were prepared and denoted as $[\text{Fe}(10.5 \text{ \AA})/\text{Ag}(14 \text{ \AA})]_n$, $[\text{Fe}(11.3 \text{ \AA})/\text{Ag}(10 \text{ \AA})]_n$, $[\text{Fe}(12 \text{ \AA})/\text{Ag}(7 \text{ \AA})]_n$, and $[\text{Fe}(15 \text{ \AA})/\text{Ag}(10 \text{ \AA})]_n$, where the number of bilayers n in the stack typically increased from $n = 1$ to 10.

In addition to the RHEED and LEED characterization, the growth of Fe(110) on Ag(111) and Ag(111) on Fe(110) also was monitored *in situ* by measurements of the 350-eV Ag Auger signal. In general, the Auger signal intensity should depend exponentially on the thickness of the deposited material. If the growth mode is layer by layer, however, the Auger signals should depend linearly on thickness within each monolayer grown and the linear segments for each species should join together to form an exponential envelope. The segmented shape and kinks at the completion of each monolayer in the Auger data in Fig. 1 suggest that the initial growth mode is layer by layer for both Fe(110) on Ag(111) and Ag(111) on Fe(110). The Fe and Ag film thicknesses shown in Fig. 1 were determined independently from a quartz-crystal thickness monitor. The thickness monitor was calibrated both by profilometry using a 2000 Å Ag film, and by SQUID magnetometry using a 100 Å Fe film and assuming that

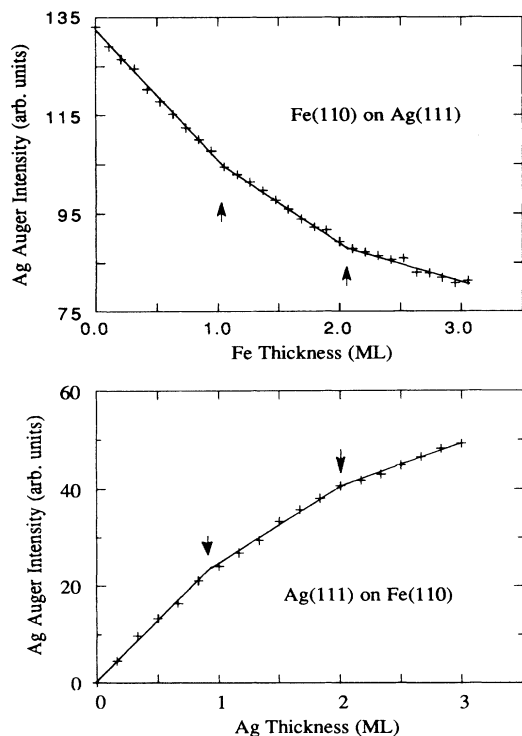


FIG. 1. The change of the Ag 350-eV Auger signal intensity during the growth of Fe(110) on Ag(111) and Ag(111) on Fe(110).

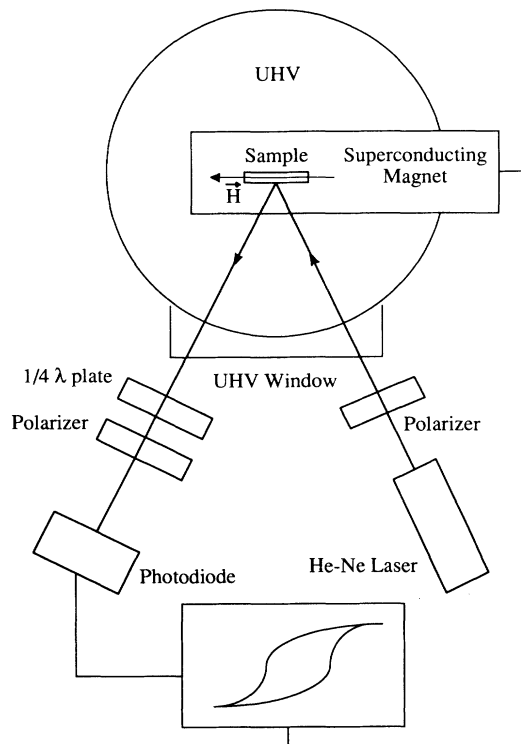


FIG. 2. A schematic of the SMOKE experiment.

the magnetic moment has the bulk value. From Fig. 1 we see that the thickness determined from the quartz-crystal monitor is consistent with the location of the Auger kinks at integral layer thicknesses.

B. SMOKE measurements

The magnetic properties of the Fe(110)/Ag(111) superlattices were measured *in situ* by means of the SMOKE technique. A schematic of the experimental arrangement is shown in Fig. 2. An intensity-stabilized, He-Ne laser was used as the light source. A linear polarizer polarized the incident light in the plane of incidence (p polarization). The angle of incidence of the light is $\sim 20^\circ$ from the surface normal. Upon reflection from the sample surface the light passes through an analyzing polarizer set at $\delta = 2^\circ$ from extinction, and a quarter-wave plate used to remove the birefringence of the UHV window. The light intensity, referred to as the Kerr intensity, is then detected by a photodiode and recorded as a function of the applied magnetic field H to generate the hysteresis loop. H was applied in the film plane and in the plane of the incident light (longitudinal Kerr effect) along the Ag $[11\bar{2}]$ direction. Due to the Kerr effect, the reflected beam (r) will have a nonzero s component of the electrical field $E_s^{(r)}$, but for which $|E_s^{(r)}| \ll |E_p^{(r)}|$. We define $E_s^{(r)}/E_p^{(r)} \equiv \phi' + i\phi''$, where ϕ' and ϕ'' are the Kerr rotation and ellipticity, respectively. In our experimental arrangement the quarter-wave plate not only eliminates the window birefringence, but also produces a 90° phase shift which interconverts rotation and ellipticity. The benefit of the signal conversion will become apparent later. Thus, the measured quantity, to first order in ϕ' and ϕ'' , is

$$I = |iE_p \sin \delta + E_s \cos \delta|^2 \approx |E_p|^2 |\delta - i\phi' + \phi''|^2 \approx |E_p|^2 (\delta^2 + 2\delta\phi'') = I_0 (1 + 2\phi''/\delta),$$

where I is the measured Kerr intensity and $I_0 = |E_p|^2 \delta^2$ is the Kerr intensity at zero net magnetization. Thus, the peak-to-peak intensity ΔI , which is the difference between the Kerr intensity at positive and negative saturation field, yields the Kerr ellipticity as follows:

$$\phi'' = \frac{\delta}{4} \frac{\Delta I}{I_0}.$$

III. RESULTS AND DISCUSSION

Figure 3 shows a typical set of SMOKE signals measured at the growth temperature of 450 K for different thicknesses of Fe(110) on Ag(111). The hysteresis loops, as shown in Fig. 3, have remanence and a low coercivity, indicative of easy axes of magnetization in the film plane, consistent with previous Mössbauer² and SMOKE¹³ observations for the Fe(110)/Ag(111) system. The Kerr ellipticity obtained from the peak-to-peak intensity is shown in Fig. 4. The Kerr signal in Fig. 4 vanishes for Fe films thinner than 1.6 monolayer (ML), and increases linearly for Fe films thicker than 4 ML. This indicates that the Curie temperature T_C is below 450 K for films thinner than 1.6 ML and is well above 450 K for films thicker than 4 ML. Detailed studies of the thickness dependence of T_C and of the critical behavior near T_C for the Fe(110)-on-Ag(111) system were reported elsewhere.¹³ In the present work, we want to concentrate primarily on the Kerr effect in Fe(110)/Ag(111) superlattices as opposed to surface phenomena, so the Fe-layer thickness are kept > 4 ML.

The Kerr signal was measured after the growth of each Fe/Ag bilayer. The ellipticity obtained from ΔI is plot-

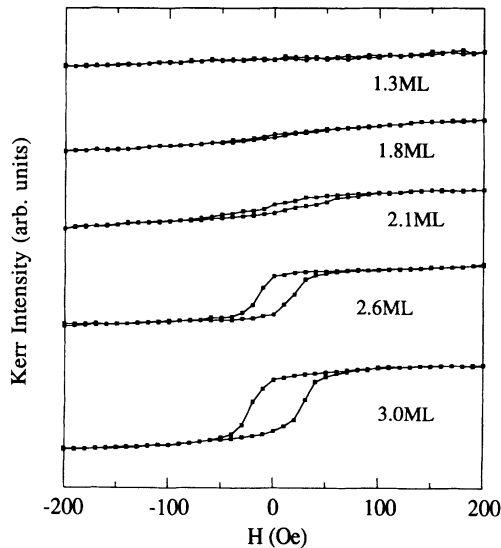


FIG. 3. SMOKE signals at 450 K for different thicknesses of Fe(110) on Ag(111).

ted in Fig. 5 as a function of the bilayer thickness. For comparison, the ellipticity measured for Fe films of different thickness on Ag is also plotted in Fig. 5. We notice that the ellipticity for each film initially increases linearly as the film thickness increases, and starts to approach saturation by ~ 100 Å thickness. The saturation effect is primarily due to the absorption of light in metals; the Kerr signal from layers well below the penetration depth are not detected.

To better understand the observed linearity of the magneto-optic signal, we follow the description of Zak *et al.*¹¹ and consider a superlattice with the film parallel to the xy plane. In a magnetic material the dielectric tensor $\tilde{\epsilon}$ has the form

$$\tilde{\epsilon} = \epsilon_0 \begin{pmatrix} 1 & iQ_3 & -iQ_2 \\ -iQ_3 & 1 & iQ_1 \\ iQ_2 & -iQ_1 & 1 \end{pmatrix},$$

where ϵ_0 is dielectric constant and $\mathbf{Q} = (Q_1, Q_2, Q_3)$ is the magneto-optic coupling or Voigt¹⁵ vector that describes the Kerr effect. Suppose that the electrical fields of the incident and reflected beams are $E_s^{(i)}, E_p^{(i)}$, and $E_s^{(r)}, E_p^{(r)}$, respectively. Then the goal becomes to find the relation between $(E_s^{(r)}, E_p^{(r)})$ and $(E_s^{(i)}, E_p^{(i)})$. The boundary conditions require that (a) in the final layer of substrate, $(E_s^{(i)}, E_p^{(i)}, E_s^{(r)}, E_p^{(r)}) = (E_s^{(t)}, E_p^{(t)}, 0, 0)$; (b) $E_x, E_y, H_x,$ and H_y are continuous at each interface of the superlattice, where the E_x, E_y and H_x, H_y are the x and y components of the electrical and magnetic fields, respectively. Zak *et al.*¹¹ have treated this problem in a general form using two types of 4×4 matrices, A and \bar{D} , referred to as the medium boundary and medium propagation matrices. These matrices relate $(E_s^{(i)}, E_p^{(i)}, E_s^{(r)}, E_p^{(r)})$ with (E_x, E_y, H_x, H_y) within each layer of the superlattice, and $(E_s^{(i)}, E_p^{(i)}, E_s^{(r)}, E_p^{(r)})$ at l th interface with (E_s, E_p, E_s, E_p)

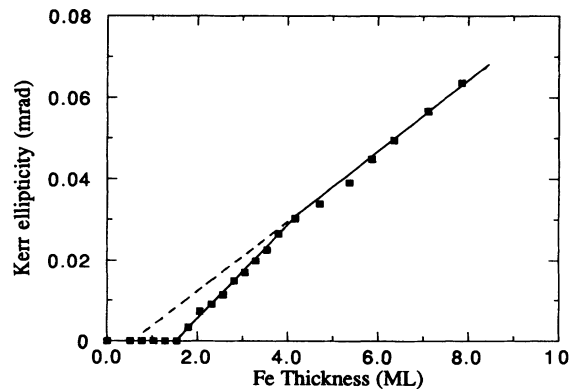


FIG. 4. Measured Kerr ellipticity at 450 K for different thicknesses of Fe(110) on Ag(111).

at the $(l+1)$ th interface, as follows:

$$\begin{pmatrix} E_x \\ E_y \\ H_x \\ H_y \end{pmatrix}_l = A_l \begin{pmatrix} E_s^{(i)} \\ E_p^{(i)} \\ E_s^{(r)} \\ E_p^{(r)} \end{pmatrix}_l$$

and

$$\begin{pmatrix} E_s^{(i)} \\ E_p^{(i)} \\ E_s^{(r)} \\ E_p^{(r)} \end{pmatrix}_l = \bar{D}_l \begin{pmatrix} E_s^{(i)} \\ E_p^{(i)} \\ E_s^{(r)} \\ E_p^{(r)} \end{pmatrix}_{l+1}$$

The boundary condition of continuity at each interface then is given by

$$A_i \begin{pmatrix} E_s^{(i)} \\ E_p^{(i)} \\ E_s^{(r)} \\ E_p^{(r)} \end{pmatrix} = \prod_l (A_l \bar{D}_l A_l^{-1}) A_f \begin{pmatrix} E_s^{(r)} \\ E_p^{(r)} \\ 0 \\ 0 \end{pmatrix}. \quad (1)$$

Here the subscripts of i and f stand for the initial and final materials, which are vacuum and Ag for the present case. After evaluating the A and \bar{D} matrices one can calculate the Kerr rotation and ellipticity.

In thin-film limit, where the total thickness of the superlattice is much less than the wavelength of the incident light, the calculation of the product of those matrices in Eq. (1) becomes greatly simplified.¹¹ The result for the p polarized, longitudinal case, which is our experimental case, is

$$\phi' + i\phi'' \equiv \frac{E_s^{(r)}}{E_p^{(r)}} = \frac{4\pi}{\lambda} \frac{n_i^2 n_f \sin\theta_i \cos\theta_i \cos\theta_f}{(n_i \cos\theta_i + n_f \cos\theta_f)(n_f \cos\theta_i - n_i \cos\theta_f)} \sum_m d_m Q_m, \quad (2)$$

where the n_i and n_f are refractive indices, and θ_i and θ_f are the angle of incidence in the initial medium and the angle of refraction in the final medium, respectively. The summation runs only over the magnetic layers and the d_m and Q_m are the thickness and the magnitude of the Q vector of the m th magnetic layer. From the above equation we see that within the thin-film limit the Kerr signal (a) depends linearly on the thickness of the magnetic component; and (b) is independent of the intervening nonmagnetic layers.¹¹

We have observed the linearity on thickness anticipat-

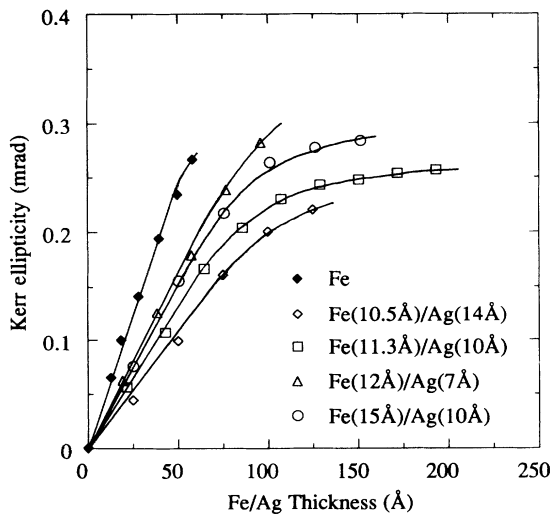


FIG. 5. Measured Kerr ellipticity of the Fe/Ag superlattices as a function of the total superlattice thickness, which is equal to $d_{\text{Fe}} + d_{\text{Ag}}$ summed over all n bilayers, or $n(d_{\text{Fe}} + d_{\text{Ag}})$. Note the initial linearity in the thin-film region.

ed from Eq. (2); it is shown in Fig. 5. To test the independence of the Kerr signal on the intervening Ag layers, we plotted the Kerr ellipticity as a function of the Fe component thickness only (Fig. 6), instead of the total bilayer thickness. Indeed, all superlattice curves fall on the same straight line as that of the pure Fe-on-Ag film. Actually, this result is quite easy to understand, since within thin-film limit the interference effect between the indivi-

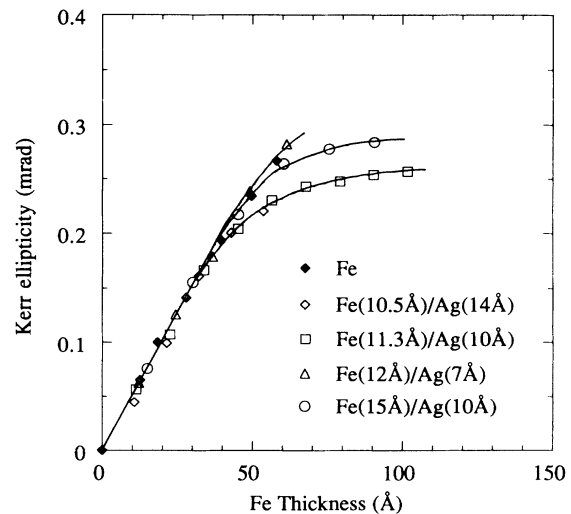


FIG. 6. Measured Kerr ellipticity of the Fe/Ag superlattices, as in Fig. 5, but plotted here as a function of the total Fe thickness only, which is equal to nd_{Fe} . All the curves initially lie on the same straight line indicating that the total Kerr ellipticity is independent of the intervening Ag layers in the superlattices. This provides experimental confirmation of the additivity law in the thin-film limit.

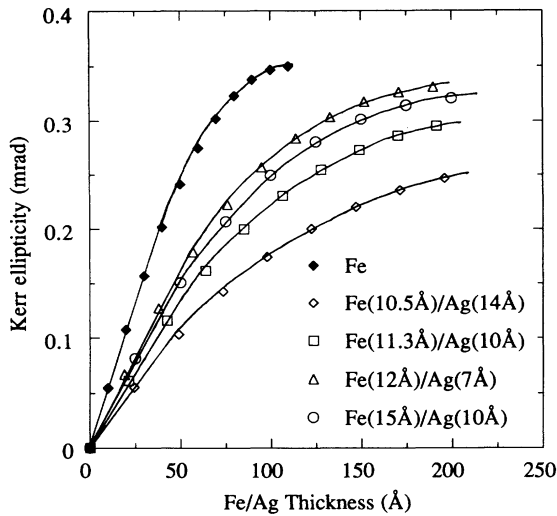


FIG. 7. Calculated Kerr ellipticity of the Fe/Ag superlattices as a function of the total superlattice thickness.

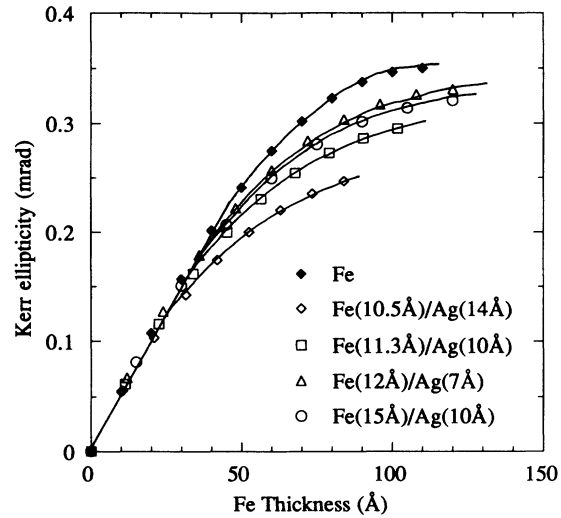


FIG. 8. Calculated Kerr ellipticity of the Fe/Ag superlattices as a function of the Fe thickness only. That the curves initially lie on the same straight line is a manifestation of the additivity law in the thin-film limit.

dual layers can be ignored so that the total Kerr signal should be just a simple summation of the Kerr signals from each individual magnetic layer. For comparison, we numerically evaluated the ellipticity for the superlattices using the full formalism of Ref. 11, by utilizing bulk values of the optical¹⁶ and magneto-optic¹⁷ constants taken from the literature; the results are shown in Figs. 7 and 8. We see that the calculated results agree very well with experiment. From the linear experimental slope in Fig. 6, we can independently evaluate the Q value for Fe from Eq. (2), and we find agreement within the 5% level with the real part of Q obtained from Ref. 16. The slight enhancement of our Q value over the literature value assumes that the difference between the slopes in Figs. 6 and 8 are solely attributable to Q and not to differences in optical constants, etc. Given that such an extreme assumption cannot be well defended, and that there are no clear alternative assumptions to make, suffice it to conclude that the level of agreement is quite good. The calculations also demonstrate the benefit of monitoring the ellipticity as opposed to the rotation, since for the thickness of interest the ellipticity is the dominant channel and the rotation gives rise to only a weak signal. This in itself is also a significant thin-film result, in that for bulk Fe the magneto-optic signal resides predominantly in the rotation channel and the ellipticity is relatively weak. A similarly prominent ellipticity was noted for ultrathin Fe grown epitaxially on Au(100).¹⁸ Thus, we find good overall agreement between our observations, previous ob-

servations, and macroscopic theory. It would be interesting to extend quantitative magneto-optic studies further toward the monolayer regime where band-structure effects and the breakdown of dielectric-response theory might be expected to lead to new properties.

IV. SUMMARY

Fe(110)/Ag(111) single-crystal superlattices were fabricated by MBE and characterized by RHEED, LEED, and Auger spectroscopy. Both Fe(110) on Ag(111) and Ag(111) on Fe(110) follow a layer-by-layer growth mode. The SMOKE technique was applied during film growth to study magnetic and magneto-optic properties of these superlattices as a function of thickness and of the number of bilayers in the film. It was found that the Kerr ellipticity initially increases linearly as a function of the Fe film thickness and is independent of the intervening Ag layers, in agreement with expectations based on the magneto-optic derivations of Zak *et al.*¹¹ evaluated in the thin-film limit.

ACKNOWLEDGMENT

This work was supported by the U.S. Department of Energy, BES-Materials Sciences under Contract No. W-31-109-ENG-38.

¹L. M. Falicov, D. T. Pierce, S. D. Bader, R. Gronsky, K. B. Hathaway, H. J. Hopster, D. N. Lambeth, S. S. P. Parkin, G. Prinz, M. Salomon, I. K. Schuller, and R. H. Victora, *J. Mater. Res.* **5**, 1299 (1990).

²W. B. Zeper, F. J. A. M. Greidanus, P. F. Carcia, and C. R. Fincher, *J. Appl. Phys.* **65**, 4971 (1989); S. Hashimoto and Y.

Ochiai, *J. Magn. Magn. Mater.* **88**, 49 (1990); S. Hashimoto, H. Matouda, and Y. Ochiai, *Appl. Phys. Lett.* **56**, 1069 (1990); K. Nakamura, S. Tsunashima, S. Iwata, and S. Uchiyama, *IEEE Trans. Magn.* **25**, 3758 (1989); S.-C. Shin and A. C. Palumbo, *J. Appl. Phys.* **67**, 317 (1990); N. K. Flevaris, *Appl. Phys. Lett.* **58**, 2177 (1991); W. A. McGahan, L.-Y.

- Chen, Z. S. Shan, D. J. Sellmyer, and J. A. Wollam, *ibid.* **55**, 2479 (1989); W. Reim and D. Weller, *IEEE Trans. Magn. MAG-25*, 3752 (1989).
- ³Z. Q. Qiu, S. H. Mayer, C. J. Gutierrez, H. Tang, and J. C. Walker, *Phys. Rev. Lett.* **63**, 1649 (1989).
- ⁴S. D. Bader, *Proc. IEEE* **78**, 909 (1990).
- ⁵S. D. Bader, *J. Magn. Magn. Mater.* **100**, 440 (1991).
- ⁶T. Katayama, H. Awano, Y. Nishihara, and N. Koshizuka, *IEEE Trans. Magn. MAG-23*, 2949 (1987); T. Katayama, Y. Suzuki, H. Awano, Y. Nishihara, and N. Koshizuka, *Phys. Rev. Lett.* **60**, 1426 (1988); **64**, 106 (1990); R. Nies and F. R. Kessler, *ibid.* **64**, 105 (1990); K. Sato, H. Kida, and T. Katayama, *Jpn. J. Appl. Phys.* **27**, L237 (1988).
- ⁷J. Zak, E. R. Moog, C. Liu, and S. D. Bader, *Appl. Phys. Lett.* **58**, 1214 (1991).
- ⁸T. Yoshino and S. Tanaka, *Jpn. J. Appl. Phys.* **5**, 989 (1966).
- ⁹W. A. McGanan and J. Woollam, *Appl. Phys. Commun.* **9**, 1 (1989).
- ¹⁰M. Mansuripur, *J. Appl. Phys.* **67**, 6466 (1990).
- ¹¹J. Zak, E. R. Moog, C. Liu, and S. D. Bader, *J. Magn. Magn. Mater.* **89**, 107 (1990).
- ¹²J. Zak, E. R. Moog, C. Liu, and S. D. Bader, *J. Magn. Magn. Mat.* **88**, L261 (1990).
- ¹³Z. Q. Qiu, J. Pearson, and S. D. Bader, *Phys. Rev. Lett.* **67**, 1646 (1991).
- ¹⁴B. Voigtländer, G. Meyer, and N. M. Amer, *Surf. Sci. Lett.* **255**, L529 (1991).
- ¹⁵W. Voigt, *Magneto-und Elektrooptik* (Teuner, Leipzig, 1908); *Handbuch der Elektrizität und des Magnetismus*, (Barth, Leipzig, 1915), Vol. IV: 2, p. 393.
- ¹⁶J. H. Weaver, in *CRC Handbook of Chemistry and Physics*, 69th edition, edited by R. C. Weast, M. J. Astle, and W. H. Beyer (CRC, Boca Raton, 1988), p. E-387ff.
- ¹⁷G. S. Krinchik and V. A. Artemev, *Zh. Eksp. Teor. Fiz.* **53**, 1901 (1967) [*Sov. Phys. JETP* **26**, 1080 (1968)].
- ¹⁸E. R. Moog, S. D. Bader, and J. Zak, *Appl. Phys. Lett.* **56**, 2687 (1990).